

Delta-sigma modulation microphone sensors employing a resonant tunneling diode with a suspended microstrip resonator

Journal:	<i>Sensor Review</i>
Manuscript ID	SR-03-2020-0044.R1
Manuscript Type:	Original Manuscript
Keywords:	delta-sigma modulator, resonant tunneling diode, ultrasonic sensor, suspended microstrip resonator

Delta-sigma modulation microphone sensors employing a resonant tunneling diode with a suspended microstrip resonator

Abstract

Purpose of this paper - We propose and demonstrate novel microphone sensors based on the frequency delta-sigma modulation (FDSM) technique, which replaces the conventional delta-sigma modulator in the delta-sigma analog-to-digital converters. A key of the FDSM technology is to employ a voltage-controlled oscillator (VCO) for converting an input analog signal to a 1-bit pulse-density modulated digital signal. High-performance sensors can be realized if the VCO is replaced by an oscillator whose oscillation frequency depends on an external physical parameter.

Design/methodology/approach - Microphone sensors are proposed based on FDSM that employs a suspended microstrip disk resonator, where the back-side ground plane is replaced by a thin metal diaphragm. A resonant tunneling diode (RTD) oscillator is also employed, as the performance of these sensors significantly depends on the oscillation frequency. To demonstrate the basic operation of the proposal, prototype devices were fabricated with an InGaAs/AlAs RTD.

Findings - A satisfactory noise shaping property, which is a significant nature of delta-sigma modulation, was demonstrated over three decades for the prototype device. A sound-sensing peak was also clearly observed when applying 1 kHz sound from a speaker.

Practical implications - High-performance ultrasonic microphone sensors can be realized if we fabricate the sensors using a thin InP substrate with high-frequency oscillator design.

What is original/value of paper - In this study, we proposed and experimentally demonstrated novel microphone sensors, which are promising as future ultrasonic sensors that have high dynamic range with wide bandwidth.

Keywords

Delta-sigma modulator, resonant tunneling diode, suspended microstrip resonator, ultrasonic sensor

1 Introduction

Delta-sigma modulation, which is a technique for performing analog-to-digital conversion (ADC), offers a wide dynamic range and high signal-to-noise ratio (SNR) without using high-precision analog components (Candy, 1974; Norsworthy *et al.*, 1996; Pavan *et al.*, 2017). A conventional delta-sigma modulator (DSM) comprises an integrator, 1-bit quantizer, and feedback digital-to-analog converter (DAC). Among them, the integrator and feedback DAC limit the sampling rate and, thus, the bandwidth. Recently, frequency DSMs (FDSMs) based on a voltage-controlled oscillator (VCO) have been attracting considerable attention (Høvin *et al.*, 1997; Iwata *et al.*, 1999; Maezawa *et al.*, 2008; Straayer *et al.*, 2008; Li *et al.*, 2019) because they require no integrator or feedback DAC and can be operated at significantly high frequencies.

FDSMs can also be used for realizing high-performance digital output sensors when the VCO is replaced by an oscillator whose oscillation frequency depends on an external physical parameter. A strain sensor and digital microphone were recently proposed by employing FDSM (Tajika *et al.*, 2016; Fujino *et al.*, 2013; Maezawa *et al.*, 2016a). Because the performance of FDSM sensors significantly depends on the oscillation frequency, using compound semiconductor high-frequency devices in the oscillator offers considerable advantages. In this study, we propose FDSM microphone sensors based on a resonant-tunneling diode (RTD) oscillator. An RTD is an ultrahigh-frequency device, and an oscillation frequency close to 2 THz has been demonstrated for RTD oscillators (Maekawa *et al.*, 2016; Asada *et al.*, 2016; Izumi *et al.*, 2017). FDSM sensors that use RTD oscillators might offer a wide frequency bandwidth, high dynamic range, and large SNR owing to their remarkable high-frequency characteristics.

This paper is organized as follows. Section 2 explains the operating principle of FDSM and its application in sensors. FDSM microphone sensors based on an RTD oscillator are also proposed using a suspended microstrip disk resonator. Section 3 describes the design, fabrication, and measured results of the prototype devices fabricated on an FR-4 PCB substrate. Finally, section 4 summarizes this paper.

2 FDSM and its application in sensors

2.1 Frequency delta-sigma modulation

In this subsection, the delta-sigma analog-to-digital converter (DSADC) and FDSM are briefly explained. Figure 1 (a) shows the basic block diagram of DSADC. It comprises a DSM and decimation filter. The DSM converts the input analog signal to 1-bit pulse-density modulated (PDM) digital signal at a sampling rate f_S , which is substantially higher than the Nyquist rate f_N . The DSM reduces the low-frequency quantization noise at the expense of its increase in high frequencies. Here, we focus on a first-order DSM, which can be easily implemented using a VCO. In this case, the quantization noise reduces by 20 dB/dec as the frequency decreases, and this is called first-order noise shaping. The decimation filter removes the high-frequency noise components of the PDM signal and converts it to multi-bit, parallel digital signals at the Nyquist rate. FDSM, which is a simple implementation of DSM, is shown in Fig. 1 (b). It

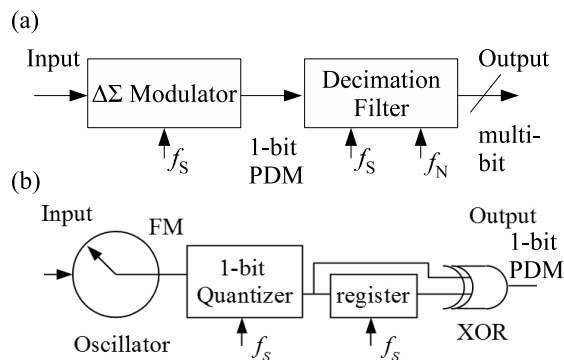


Figure 1: Block diagram of the delta-sigma ADC (a), and the FDSM (b).

comprises a VCO, whose oscillation frequency depends on the input signal, and a small digital circuit that functions as an edge detector. The VCO converts the input analog signal to a frequency-modulated (FM) signal, and the edge-detector circuit outputs pulses when the FM signal crosses zero. Because of the nature of an FM signal, a first-order DSM can be implemented using this simple circuit (Høvin *et al.*, 1997). FDSM offers a significant advantage in that it does not have any feed-back loop, which limits the operating frequency of conventional DSMs.

FDSM is also promising in sensor applications. By replacing the VCO with an oscillator whose oscillation frequency depends on an external physical parameter, **it can be used for a sensor integrated with an ADC**. The performance of this sensor depends on the frequency modulation width of the oscillator and sampling frequency. Generally, the frequency modulation ratio to the sensing parameter variation is constant, and thus increasing the oscillation frequency is advantageous. **Additionally, using a higher-frequency oscillator offers various advantages, including wide frequency bandwidth and small area**. Consequently, applying RTD oscillators to these sensors provides significant advantages.

2.2 Microphone sensors based on a suspended microstrip disk resonator

We propose microphone sensors that are based on a suspended microstrip disk resonator. Figure 2 depicts the diagram of the suspended microstrip resonator for the proposed sensor, as well as the current distribution on the resonator. The disk-shaped resonator works similar to a $\lambda/4$ transmission line, as shown in the current distribution. **This circuit can be considered a simple LC-parallel, negative-resistance oscillator because the disk resonator functions as an LC-parallel circuit near the resonant frequency. The RTD acts as a negative resistor and oscillates at the resonant frequency of the disk resonator. Here, we choose the disk-type resonator, as it has a small characteristic impedance with a large Q-factor owing to its good symmetry.** The small characteristic impedance ensures harmonic (sinusoidal) oscillation rather than relaxation oscillation when connected to the RTD (Tajika *et al.*, 2016; Maezawa *et al.*, 2016b). Compared with relaxation oscillation, harmonic oscillation offers a significant advantage of

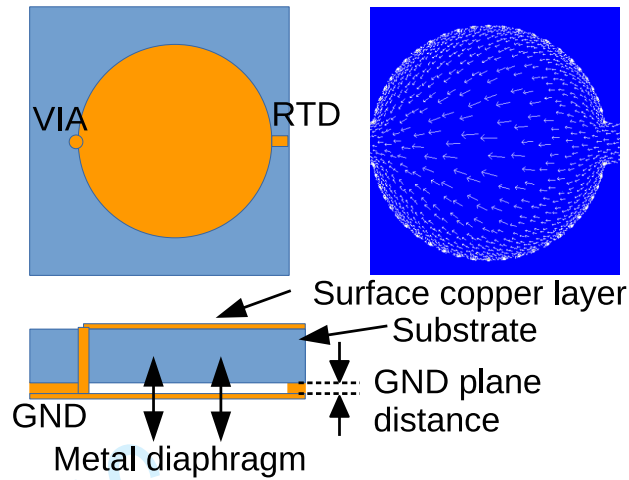


Figure 2: Basic structure of the suspended microstrip resonator based ultrasound sensor using an RTD. (Upper left: top view; lower left: cross-sectional view; right: current distribution of the resonator.

improving the phase noise property. Moreover, a significantly high Q-factor of the disk resonator improves the phase noise, which determines the noise floor of the output data. We inserted a via at the end of the disk to ensure the dc-grounding of the RTD. The key is to replace the backside ground plane with a thin metal diaphragm, which is set apart from the dielectric substrate. The signal-propagation velocity of the (suspended) microstrip line is inversely proportional to the $\sqrt{\epsilon_{\text{eff}}}$, where ϵ_{eff} denotes an effective dielectric constant. In the case of the suspended microstrip, the effective dielectric constant is approximated as

$$\epsilon_{\text{eff}} = \frac{\epsilon_{\text{sub}}\epsilon_0}{\epsilon_0 d_{\text{sub}} + \epsilon_{\text{sub}}d} (d_{\text{sub}} + d). \quad (1)$$

where ϵ_{sub} , d_{sub} , and d denote the dielectric constant of the substrate, thickness of the substrate, and GND plane distance, respectively. Consequently, the resonant frequency also significantly depends on the GND plane distance.

We performed electromagnetic-field simulation using Keysight EMPro to clarify the dependence of the resonant frequency on the GND plane distance in the case of the suspended microstrip disk based resonators on an InP substrate. An example of the calculated resonant frequency is shown in Fig. 3. The disk diameter was chosen to be $1800 \mu\text{m}$, and the substrate thickness was $450 \mu\text{m}$. The oscillation frequency for the GND plane (diaphragm) distance of $0 \mu\text{m}$, which corresponds to the microstrip resonator, was 9.25 GHz . A low resonant frequency was chosen in this example to suppress the effects of the substrate mode. The substrate mode is a resonant mode of the electromagnetic wave in a substrate perpendicular to the surface. For example, the quarter of the wavelength of a 47-GHz electromagnetic wave is equal to the InP-substrate thickness, significantly affecting the S-parameter of the resonator and hindering appropriate oscillation. The resonant frequency increases with the GND plane distance because of decrease in the effective dielectric constant, thereby resulting

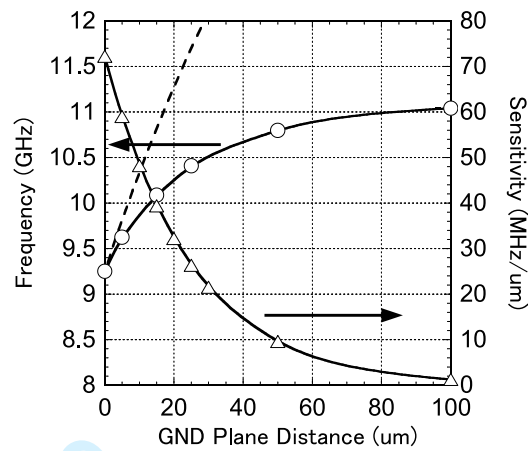


Figure 3: Example of the calculated resonant frequency and sensitivity of the suspended-disk-shaped resonator fabricated on an InP substrate. The resonator diameter is $1800 \mu\text{m}$, and the substrate thickness is $450 \mu\text{m}$. The dashed line shows the resonant frequency for the two-layer dielectric model expressed in equation (1).

in higher signal velocity. The result for the two-layer dielectric model shown in equation (1) is also plotted for reference. As depicted in the figure, this simple model is valid only for small GND plane distances, and it rapidly deviates from the electromagnetic-simulation result. This deviation is attributed to the edge effect, in which the electromagnetic field spreads out of the disk.

This figure also shows the sensitivity of the sensor. The sensitivity is defined as the derivative of the resonant frequency with respect to the GND plane distance. It increases as the GND plane distance decreases. For example, the sensitivities of 50 and 10 $\text{MHz}/\mu\text{m}$ were obtained for the distances of 10 and 50 μm , respectively. These values are significantly higher than that of a cylindrical cavity resonator sensor, i.e., $0.27 \text{MHz}/\mu\text{m}$ (Maezawa *et al.*, 2016a). Such high sensitivities are essential for high-performance sensors. In addition, this sensor structure is advantageous for integration process.

Upon reducing the substrate thickness, a resonator with higher frequency can be used **without interference with the substrate mode**. Figure 4 shows such an example. It depicts the simulation results for a resonator fabricated on a $50\text{-}\mu\text{m}$ -thick InP substrate. The resonator diameter was chosen to be $200 \mu\text{m}$, meaning that the aspect ratio is the same as that for the previous model. The resonant frequency for the microstrip resonator was 94.6GHz , and it increased while moving the GND plane further from the backside of the substrate. Using this thin substrate, a significant variation that exceeded 100% was observed in the resonant frequency for the GND plane motion of $100 \mu\text{m}$. Because of this substantial variation, the sensitivity became considerably higher than that in Fig. 3. Notably, the sensitivities of 3000 and 400 $\text{MHz}/\mu\text{m}$ are expected for the GND plane distances of 10 and 50 μm , respectively. Additionally, such a significant variation in the oscillation frequency is possible for RTD oscillators because RTDs show a nearly constant negative differential conductance for up

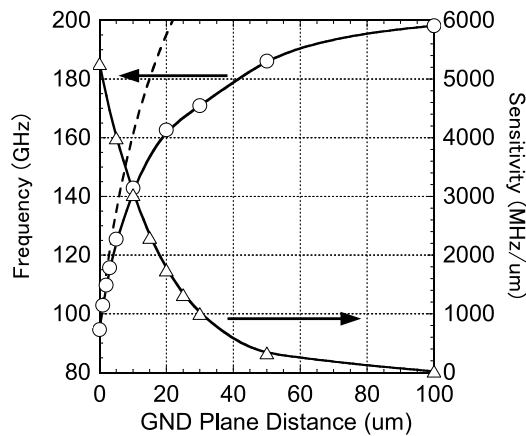


Figure 4: Example of the sensitivity calculated for the suspended-disk-shaped resonator fabricated on an InP substrate. The resonator diameter is $200 \mu\text{m}$, and the substrate thickness is $50 \mu\text{m}$. The dashed line represents the resonant frequency for the two-layer dielectric model described in equation (1).

to the THz frequency range.

Here, we compare our proposal with MEMS capacitive microphones (Shah *et al.*, 2019; Zawawi *et al.*, 2020), which are widely used because of their high sensitivity, flat frequency response, and low noise levels. The sensitivity of capacitive microphones is defined as the output voltage swing for the sound pressure of 1 Pa, and it ranges between a few mV/Pa and few tens of mV/Pa. Another important figure of merit, i.e., SNR, is defined for the sound pressure of 1 Pa and ranges between 60 and 70 dB for the bandwidth of 20 kHz. The definition of the sensitivity of our device is fairly different than that of an MEMS capacitive microphone, and thus it is difficult to directly compare them. Instead, we compare them in terms of SNR. Notably, the SNR of FDSM can be expressed as (Høvin *et al.*, 1997) follows:

$$\text{SNR} = 20 \log \left(\frac{\Delta f}{f_s \sqrt{2}} \right) - 20 \log \left(\frac{\pi}{6} \left(\frac{2f_{\max}}{f_s} \right)^{3/2} \right), \quad (2)$$

where Δf , f_s , and f_{\max} denote the maximum deviation in the frequency, sampling rate, and bandwidth, respectively. Assuming that the diaphragm-motion amplitude is $0.5 \mu\text{m}$ for the sound pressure of 1 Pa, as that for a typical MEMS microphone, we obtain a high SNR of 107 dB for the device shown in Fig. 3 while assuming a sampling rate of 12.6 GHz. The SNR can be further increased to 153 dB for the device shown in Fig. 4 while assuming a sampling rate of 126 GHz. These high SNRs indicate the promise shown by FDSM microphones. Moreover, FDSM microphones offer an important advantage in that they do not suffer from pull-in instability. This instability occurs in MEMS capacitive microphones when the applied voltage exceeds a critical value, and thus the electric field snaps the diaphragm down to the back plate. This restricts the maximum voltage, minimum air-gap, and, hence, sensitivity. Because an FDSM microphone requires no DC bias, it does not suffer from pull-in instability.

1
2
3
4
5
6
7
8 Finally, we comment on the amplitude of the diaphragm motion under a
9 sound pressure. Upon reducing the device size to increase the frequency, the
10 diaphragm-motion amplitude also decreases. However, the diaphragm size is
11 independent of disk size, and one can shrink the disk while maintaining the
12 diaphragm diameter. Moreover, the GND plane distance can be reduced without
13 the risk of pull-in instability to compensate for a small diaphragm motion.

14 Consequently, the oscillators that use suspended microstrip resonators with
15 an RTD might show significantly high sensitivity and are thus promising for use
16 in microphone sensors. Especially, such high-frequency oscillators are promising
17 for use in ultrasonic sensors.

19 3 Demonstration of the basic operation using 20 prototype devices

21
22 Fabricating the sensor using an InP substrate requires precise and cumbersome
23 processes, including substrate thinning, via-hole construction, and diaphragm
24 formation. Here, we fabricated prototype devices using an FR-4 PCB substrate
25 with InGaAs/AlAs RTD chip. Although these devices have lower sensitivity
26 than that of the above-mentioned sensors because of their lower oscillation fre-
27 quency and lower dielectric constant, they can perform the basic operation and
28 provide us with fundamental data to discuss their performances.

31 3.1 Prototype device structure and fabrication process

32 Figure 5 depicts the structure and circuit diagram of the prototype device we
33 fabricated. We used a 0.8-mm-thick FR-4 PCB substrate, whose dielectric con-
34 stant was approximately 4.5 at 1 GHz. The thickness of the surface copper
35 layer was 18 μm . The RTDs were prepared as follows. First, the epitaxial layers
36 were grown via molecular-beam epitaxy on a GaAs substrate with metamorphic
37 buffer layer (Maezawa *et al.*, 2005). The RTDs were then fabricated via con-
38 ventional photolithography and the lift-off process. Subsequently, a $2.5 \times 2.5 \text{ mm}^2$
39 RTD chip was cut out from the substrate and bonded to the FR-4 substrate.
40 Al wires with the diameter of $25 \mu\text{m}$ were used to connect the RTD pads to the
41 copper lines on the PCB. The parameters of the fabricated RTD are listed in
42 Table 1. The metal diaphragm was made of a commercial, 12- μm -thick Al-foil.
43 The disk diameter was 20 mm, which corresponds to the resonant frequency of
44 1.25 GHz when the backside metal completely contacts the substrate (microstrip
45 case). This low frequency of 1.25 GHz was chosen to eliminate the influence of
46 bonding wires. The FR-4 substrate was processed using a PCB milling ma-
47 chine so that the backside of the disk resonator could be slightly thinned while
48 removing the copper. The ventilators were fabricated around the resonator to
49 eliminate the effects due to variation in the ambient air pressure. The oscillator
50 comprised a disk resonator and an RTD connected in series. The bias terminal
51 of the RTD was grounded using a 5- Ω resistor to suppress spurious oscillations.
52 An image of the fabricated device is shown in Fig. 6.

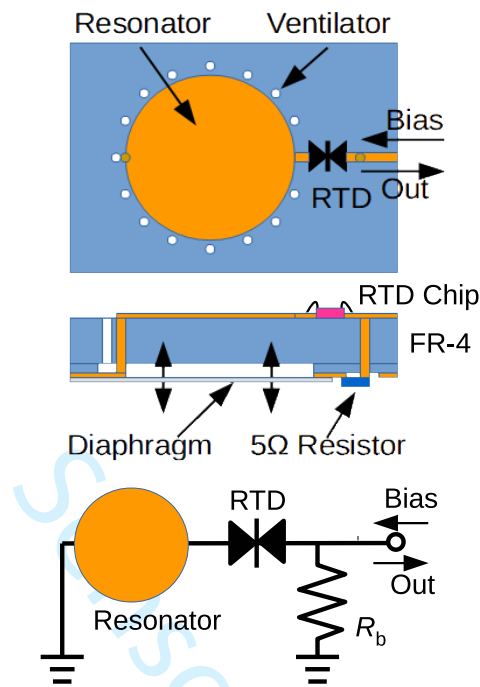


Figure 5: Structure and circuit diagram of the sensor fabricated using an RTD.

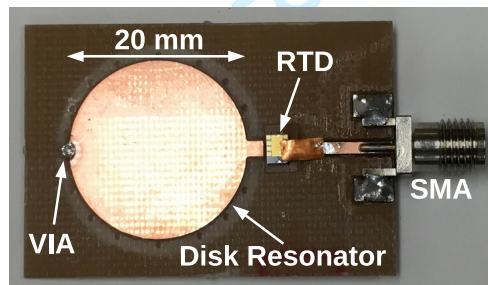


Figure 6: Fabricated sensor. The stabilizing resistor, R_b , is on the backside of the substrate.

Table 1: Parameters of the RTD used in the experiment.

Peak voltage	0.67 V
Peak current density	1.0×10^5 A/cm ²
Area	18 μm^2
Peak/valley ratio	6

3.2 Microstrip resonator oscillator

First, we tested an oscillator without a diaphragm, but with a backside GND plane that contacted the substrate, for reference. The oscillating frequency of

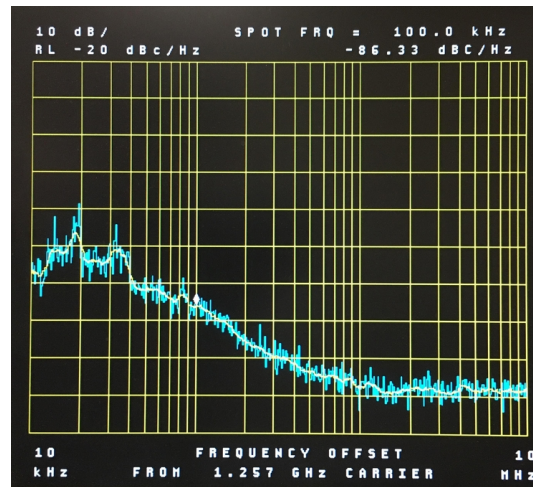


Figure 7: Phase noise property of the fabricated microstrip disk resonator oscillator.

the oscillator was approximately 1.25 GHz, which was stable against changes in the bias voltage (less than 0.05 GHz over the bias-voltage range of 0.7–1.2 V). This implies that the harmonic-type oscillation occurred because the relaxation-type oscillation significantly depends on the bias voltage (Tajika *et al.*, 2016). Next, we measured the phase noise property of the oscillator, as shown in Fig. 7. A low phase noise of -86 dBc/Hz was obtained at 100 kHz apart from the carrier frequency.

3.3 Experimental setup for sound sensing

Figure 8 shows the setup of the sound-sensing experiment. The bias voltage was applied via a bias-tee, and the oscillation signal was also taken out from the bias-tee. The signal was amplified using an RF amplifier (Keysight 83017A) and fed to a signal analyzer that was constructed on a field-programmable gate array (FPGA) chip. A 2-GHz, low-pass filter was inserted between the amplifier and signal analyzer. It was essential because the output of the oscillator was taken from the bias port. Accordingly, the output voltage was proportional to the RTD current, which has strong harmonics because of the strong non-linear I - V characteristics of RTD, although the oscillation in the resonator is sinusoidal.

The signal-analyzer circuit was constructed on an FPGA evaluation board, called Xilinx ZCU-102 (XC7K325T-2FFG900C). Its block diagram is shown in Figure 9. It comprises a high-frequency sampler, an edge detector, and a digital-filter. A high-frequency transceiver module was used for the sampling circuit, which could be operated at the sampling rate of as high as 16.3 Gb/s. Here, the sampling rate was chosen to be 12.582912 Gb/s, which corresponds to the oversampling ratio of 65536 for a signal bandwidth of 96 kHz.

The sampled 1-bit digital signal was converted to a 32-bit parallel data stream and then fed to the edge detector, which comprised XORs and registers. Subsequently, the 32-bit PDM data stream was compressed to a 6-bit data

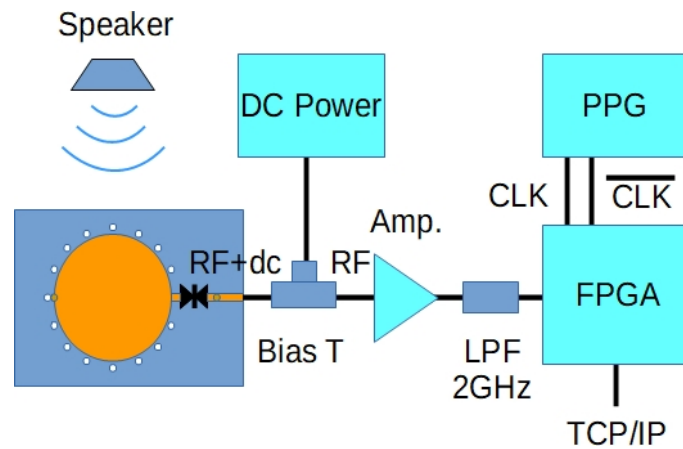


Figure 8: Measurement setup of the sound-sensing experiments.

stream by counting “1”. This works as a moving average LPF. Next, the 6-bit data stream was fed to the cascaded integrator–comb (CIC) filter, which functioned as a sinc2 filter, to eliminate high-frequency noise components and convert the signal to a 32-bit output data stream at the Nyquist rate. The filter module is shown in the lower illustration in Fig. 9. The output data were transferred to the random access memory by using a direct memory access (DMA) module. Finally, the output signal was displayed on a PC. When we tested the noise shaping property, the output of the edge detector was directly transferred to the memory.

3.4 Results and discussion

To check the natural gap between the substrate and diaphragm, we first attached a fixed and flat GND plane (copper-covered PCB) to the backside of the substrate, following which we measured the oscillation frequency. The circuit oscillated at approximately 1.63 GHz. We compared this oscillation frequency with that of the electromagnetic-simulation result and obtained a gap of approximately 0.15 mm, which was significantly larger than the copper-layer thickness of 18 μm . This gap corresponded to the scraped depth of the substrate when the backside copper was removed using the PCB milling machine.

Next, the fixed GND plane was replaced by a 12- μm -thick Al-foil. The oscillation frequency was approximately 1.54 GHz, which was slightly smaller than that of the fixed GND plane. This difference is probably because of the distortion of the Al-foil.

Subsequently, we measured the response of the fabricated sensor to an audio sound signal generated from a speaker. Figure. 10 shows the noise shaping property. This is a fast Fourier transformation (FFT) result of the 1-bit PDM digital signal, which was directly taken from the edge detector. The Blackman–Harris window was used for the FFT. **A clear noise-shaping behavior was observed over three decades, thereby demonstrating an appropriate delta-sigma operation. However, the slope gradually decreased for frequencies less than 10 MHz, and a noise floor was observed at the frequencies lower than 1 MHz. This noise**

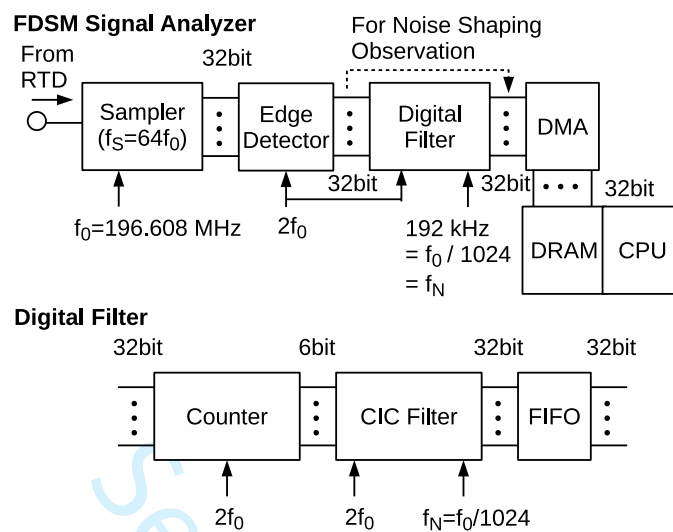


Figure 9: Block diagram of the signal-analyzer circuit on an FPGA. The lower illustration details the digital filter, which eliminates the high-frequency noise components and converts the PDM signal to a 32-bit parallel signal at the Nyquist rate.

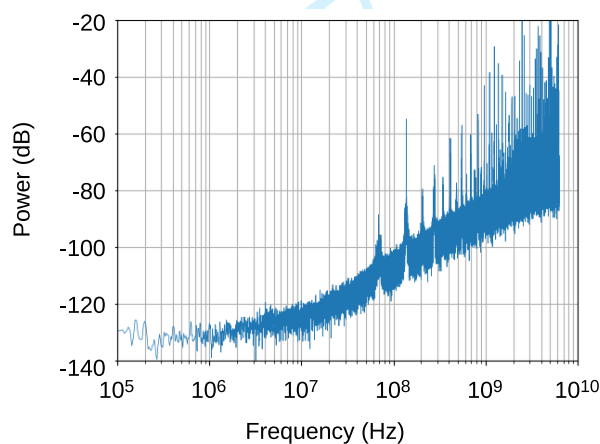


Figure 10: Example of the FFT result of the output 1-bit digital signal, which was obtained immediately after edge detection. Four data series were averaged for this plot.

floor is attributed to the phase noise of the oscillator resulted form the significant dielectric loss of the FR-4 substrate. This should be improved using an InP substrate. Furthermore, many peaks are visible at frequencies higher than 100 MHz. They are probably attributed to the pattern noise.

An example of the FFT results for the output 32-bit data stream at the

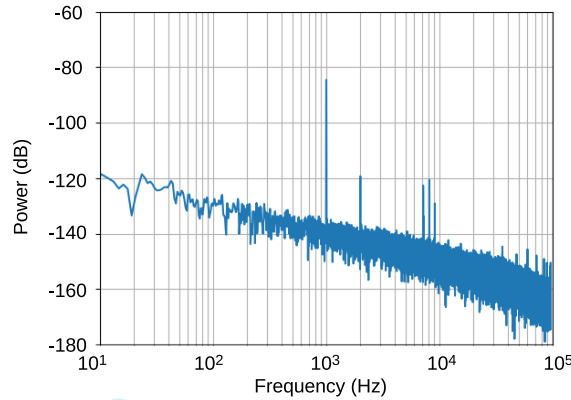


Figure 11: Example of the FFT results of the digital output stream from the digital filter. A 1-kHz sound signal with 114 dB SPL was applied to the sensor. The frequency band width was 96 kHz, and hence the Nyquist rate was 192 kHz.

Nyquist rate (192 kHz) is shown in Fig. 11. Here, we used a special type of speaker, a calibrator for sound-level meter. It could apply a 1-kHz sound with an accurate pressure of 114 dB SPL when hermetically connected to the microphone. A clear sound-signal peak was observed at 1 kHz; the peak-to-peak frequency modulation amplitude was approximately 500 kHz for this peak. The electromagnetic simulation of this device revealed that its sensitivity was $0.94 \text{ MHz}/\mu\text{m}$, which indicated that the average diaphragm-vibration amplitude was approximately $0.5 \mu\text{m}$. FDSM sensors can handle this small motion of the diaphragm with a wide bandwidth. Notably, the small vibration amplitude of this device is attributed to the thick Al diaphragm, and it can be enhanced further using a thinner diaphragm.

It is noted here that one must consider the skin depth when reducing the diaphragm thickness. The microwave electromagnetic field penetrates a metal at skin depth. The diaphragm thickness should be a few times greater than the skin depth to confine the electromagnetic waves. Because the skin depth of the Al-film is $2.2 \mu\text{m}$ for 1.5 GHz, we can reduce the thickness by half. Moreover, we can further reduce the thickness to less than $1 \mu\text{m}$ upon using higher frequencies, as the skin depth is inversely proportional to the square root of frequency. Thus, we can improve the sensitivity and enable the detection of a significantly low pressure.

The sensitivity to the unit motion of the diaphragm is also significantly lower than the values discussed in Section 2. This is attributed to the low dielectric constant of the PCB substrate, large gap, and low oscillation frequency. A considerable peak height, for example, 60-dB higher peak, can be expected upon using the $50\text{-}\mu\text{m}$ -thick InP substrate. Moreover, using the InP substrate offers another advantage, i.e., of reduced noise floor. The Q-factor of the resonator significantly depends on the dielectric loss tangent ($\tan \delta$). The $\tan \delta$ of InP is approximately 0.001, while that of FR-4 is 0.01. Therefore, we ex-

pect a reduction of 20 dB in the phase noise and that of 20 dB in the noise floor. Consequently, significantly high performance is expected using the InP substrate.

Throughout the experiment, the dc-bias voltage was set to 1.0 V, which corresponds to the power consumption of approximately 10 mW in the RTD. However, the bias-stabilization resistor R_b unnecessarily consumes a significantly higher power of 200 mW, which can be eliminated using hard-type oscillator technique (Maezawa *et al.*, 2018; Narahara and Maezawa, 2005).

Finally, we comment on the non-linearity of this sensor. FDSM-type ADCs suffer from VCO non-linearity. In this application, we observed no noticeable degradation due to the non-linearity. (The 2nd harmonic peak in Fig. 11 should be attributed to the speaker because other microphones also show this peak.) This is because the frequency modulation amplitude is only approximately 0.03% of the oscillation frequency. However, this small ratio renders the sensitivity low. This can be easily increased by increasing the oscillation frequency while maintaining the modulation ratio as low. This is one of the most important advantages of using high-frequency oscillators.

4 Conclusion

FDSM microphone sensors were proposed using an RTD oscillator. First, we discussed the advantages of the FDSM technique for realizing high-performance sensors, as well as the advantages of using RTD oscillators in FDSM sensors. The microphone sensors that used a suspended microstrip disk resonator were proposed based on the above discussion. The backside ground plane of the suspended microstrip resonator was replaced by a thin metal diaphragm, which modulated the oscillation frequency of the RTD oscillator. Through electromagnetic-field simulation, we demonstrated that high sensitivity of the oscillation frequency to the diaphragm motion could be obtained with these structures.

A prototype device was fabricated on an FR-4 PCB substrate using an In-GaAs/AlAs RTD. To demonstrate the FDSM operation, we constructed an FPGA-based signal-analyzer circuit, which could sample the output of the RTD oscillator with the sampling rate as high as 16.3 GS/s. Using this signal analyzer, a satisfactory noise shaping property over three decades and sound sensing were demonstrated for the prototype device. In conclusion, high-performance ultrasound microphone sensors should be realized using thin InP substrates with high-frequency oscillators.

References

- Asada, M., and Suzuki, S., (2016), "Room-Temperature Oscillation of Resonant Tunneling Diodes close to 2 THz and Their Functions for Various Applications," *J. Infrared Milli Terahertz Waves*, DOI 10.1007/s10762-016-0321-6.
- Candy, C., (1974), "A Use of Limit Cycle Oscillations to Obtain Robust Analog-to-Digital Converters," *IEEE Trans. on Commun.*, vol. 22, no. 3, pp. 298-305.
- Fujino, S., Mizuno, Y., Takaoka, K., Nakano, J., Mori, M., and Maezawa, K., (2013), "Experimental Demonstration of Noise Shaping in the Digital Microphone Employing Frequency $\Delta\Sigma$ Modulation," *IEICE Trans. Electron. (Japanese Edition)*, Vol. J96-C, No. 12, pp. 554-555.

- 1
2
3
4
5
6
7
8 Høvin, M., Lande, T. S., Toumazou, C. (1997), "Delta-Sigma Modulators Using Frequency-
9 Modulated Intermediate Values," *IEEE J. Solid-State Circuits* 32, pp. 13–22.
- 10 Iwata, A., Sakimura, N., Nagata, M., and Morie, T., (1999), "The Architecture of Delta Sigma
11 Analog-to-Digital Converters Using a Voltage-Controlled Oscillator as a Multibit Quantizer,"
12 *IEEE Trans. Circuits and Systems-II* 46, pp. 941–945.
- 13 Izumi, R., Suzuki, S., and Asada, M., (2017), "1.98 THz Resonant-Tunneling-Diode Oscillator
14 With Reduced Conduction Loss By Thick Antenna Electrode," *Int. Conf. Infrared, Millimeter,
15 and Terahertz waves (IRMMW-THz)*, MA3.1, Cancun, Mexico.
- 16 Li, S., Sanyal, A., Lee, K., Yoon, Y., Tang, X., Zhong, Y., Ragab, K., and Sun, N., (2019), "Advances
17 in Voltage-Controlled-Oscillator-Based $\Delta\Sigma$ ADCs," *IEICE TRANS. ELECTRON.*, VOL.E102-C,
18 NO.7, pp. 509-519.
- 19 Maekawa, T., Kanaya, H., Suzuki, S., and Asada, M., (2016), "Oscillations up to 1.92 THz in
20 resonant tunneling diode by reduced conduction loss," *Appl. Phys. Exp.*, vol. 9, 024101.
- 21 Maezawa, K., Fujino, S., Yamaoka, T., and Mori, M., (2016a), "Delta Sigma Modulation Micro-
22 phone Sensors Using a Microwave Cavity Resonator," *Electron. Lett.* 52, pp. 1651-1652. DOI:
23 10.1049/el.2016.2538
- 24 Maezawa, K., Iwase, T., Ohno, Y., Kishimoto, S., Mizutani, T., Sano, K., Takakusaki, M., and
25 Nakata, H., (2005), "Metamorphic Resonant Tunneling Diodes and Its Application to Chaos
26 Generator ICs," *Jpn. J. Appl. Phys.*, Vol. 44, No. 7A, pp. 4790-4794.
- 27 Maezawa, K., and Mori, M., (2016b), "Impulse Sensitivity Function Study of the Phase Noise in
28 Resonant Tunneling Diode Oscillators," *Asia-Pacific Workshop on Fund. and Appl. Semicond.
29 Dev. (AWAD2016)*, Hakodate, Japan.
- 30 Maezawa, K., and Mori, M., (2018), "Possibilities of Large Voltage Swing Hard-Type Oscillators
31 Based on Series-Connected Resonant Tunneling Diodes," *IEICE Trans. Electron.*, Vol.E101-C,
32 No. 5, pp. 305-310.
- 33 Maezawa, K., Sakou, M., Matsubara, W., and Mizutani, T., (2006), "Resonant tunneling delta-
34 sigma modulator suitable for high-speed operation," *Electron. Lett.* 42, 20063215.
- 35 Narahara, K., and Maezawa, K., (2018), "Characterization of a hard-type oscillator using
36 series-connected tunnel diodes," *IEICE Electron. Express*, Vol. 15, No. 10, pp. 1-6. DOI:
37 10.1587/elex.15.20180355
- 38 Norsworthy, S. R., Schreier, R., Temes, G. C. (1996), *Delta-Sigma Data Converters*, IEEE Press,
39 New York, USA.
- 40 Shah, M. A., Shah, I. A., Lee, D.-G., and Hur, S., "Design Approaches of MEMS Microphones for
41 Enhanced Performance", *Journal of Sensors*, Vol. 2019, 9294528, DOI: 10.1155/2019/9294528
- 42 Pavan, S., R., Schreier, R., Temes, G. C. (2017), "Understanding Delta-Sigma Data Converters
43 (2nd Ed.)," *Wiley & Sons, New Jersey, USA.*
- 44 Straayer, M. Z., and Perrott, M. H., (2008), "A 12-bit, 10-MHz bandwidth, continuous-time ADC
45 with a 5-bit, 950-MS/s VCO-based quantizer," *IEEE J. Solid-State Circ.* 43, p. 805.
- 46 Tajika, T., Kakutani, Y., Mori, M., and Maezawa, K., (2016), "Experimental demonstration of
47 strain detection using resonant tunneling delta-sigma modulation sensors," *Phys. Status Solidi*,
48 A 214, No. 3, 1600548. DOI: 10.1002/pssa.201600548
- 49 Zawawi, S. A., Hamzah, A. A., Majlis, B. Y., and Mohd-Yasin, F., (2020), "A Review of MEMS
50 Capacitive Microphones," *Micromachines*, 2020, 11, 484, doi:10.3390/mi11050484
- 51
52
53
54
55
56
57
58
59
60